FARADAY

Bluemoon simulations of benzene in silicalite-1

Prediction of free energies and diffusion coefficients

Timothy R. Forester and William Smith*†

DCI, CCLRC Daresbury Laboratory, Daresbury, Warrington, Chesire, UK WA4 4AD

Constrained reaction coordinate (Bluemoon) dynamics have been used to characterise the free energy profile of benzene in silicalite-1 at 300 K along the mean reaction path for diffusion. The reaction path was found empirically by fitting a parametric curve through the mean positions of the benzene centre of mass. Both rigid and flexible zeolite lattices have been investigated. In both cases the primary adsorption site was located at the intersection of the straight and sinusoidal channels. Two other distinct adsorption sites exist in the straight channel and four in the sinusoidal channel. Lattice flexibility was found to have a very strong influence on the relative free energies of the adsorption sites and on the free energies of the transition states connecting them. The free energies, combined with estimates of the transmission coefficient, κ, were used to obtain rate constants for diffusion between the main adsorption sites in the flexible lattice. Subsequent diffusive Monte Carlo simulations, using these parameters, provided the self-diffusion coefficient, D, and its components, at 300 K. We obtained $D = 3.36 \times 10^{-14}$ m^2 s^{-1}, in excellent accord with the best experimental value of 2.2×10^{-14} m^2 s^{-1}. Diffusion was fastest in the Y direction with the $D_{yy}/D_{xx} = 1.49$ and $D_{yy}/D_{zz} = 5.65$ being observed.

The synthetic zeolite ZSM5, and its purely siliceous form, silicalite, are among the most studied of all zeolites. The structure of this microporous material consists of straight channels intersected by slightly narrower sinusoidal channels (Fig. 1). What makes this of particular interest is that the channels (internal diameter *ca.* 5.5 Å) are just large enough to accommodate a benzene ring and consequently the diffusion of alkylated aromatics through this zeolite attenuates rapidly as larger substituents are added to the phenyl ring. This 'shape-selectivity' makes ZSM5 extremely important in the petrochemical industry. For example, in xylene isomerization over ZSM5 the product distribution is biased towards the isomer with the highest diffusion coefficient (*viz. p*-xylene), which also happens to be the most commercially valuable isomer.[1] The product distribution in such reactions is, to a large extent, determined by the relative diffusion coefficients of the species concerned. There is, thus, considerable interest in understanding and predicting the transport of aromatics in shape-selective catalysts such as ZSM5. However, the diffusion rates of aromatics in zeolites are low and, to date, the best theoretical studies compare only moderately well with the best experimental measurements.[2] Benzene adsorbed in silicalite is one such system. Experimental measurements are consistent with the benzene residing at a number of adsorption sites with infrequent hops made between them.[3–5]

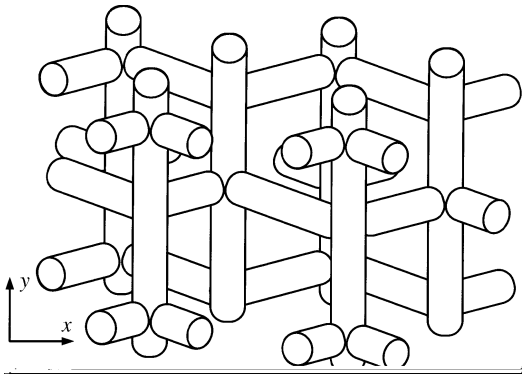

Fig. 1 Schematic diagram of the ZSM-5 and silicalite channel structure. The straight and sinusoidal channels have internal diameters of *ca.* 5.5 Å. The spacing along the straight channel between adjacent sinusoidal channels is *ca.* 10 Å. Diffusion in the Z direction is only possible by paths involving a combination of both straight and sinusoidal channels.

There has been intense effort given to calculating the adsorption and diffusion properties of hydrocarbons and other adsorbates in zeolites. Many of the previous studies of diffusion of hydrocarbons in silicalite (and other zeolites) have focused on small linear alkanes where the diffusion rates are relatively fast (see *e.g.* ref. 6–8) but even with molecules like hexane, simulation times approaching nanoseconds are required to obtain meaningful statistics.[8] The situation for benzene in silicalite is worse: the experimental diffusion coefficient at room temperature is 2.2×10^{-14} m^2 s^{-1} (fitted from the data of ref. 9–11) making reliable estimates by conventional molecular dynamics unfeasible. A simulation of *ca.* 30 μs would be required for an average displacement of the benzene by just one unit cell length in the [010] direction. Alternative methods have thus been sought.

Early attempts mapped out the adsorption energy of benzene as a function of its position and orientation in a rigid zeolite matrix.[12] Estimates for the activation energy for diffusion could thus be obtained. Attention then turned to tracing out minimum-energy paths[13,14] and using transition-state theory (TST) to obtain the diffusivity.[15,16] The most thorough TST calculation located 27 potential-energy minima and 100 distinct transition states in the asymmetric unit cell.[16] Diffusive paths were mapped out connecting these minima and rate constants for each path estimated using a harmonic approximation for the entropy at each transition point. Many of the minima lay close to each other and were separated only by small barriers. They may, thus, be grouped into a much smaller number of adsorption 'macrostates' consistent with experimental data.

An alternative, and potentially much more efficient, approach is to use molecular dynamics in the constrained reaction coordinate dynamics (CDRC) ensemble, also known as the 'Bluemoon' ensemble, since it caters for statistically rare phenomena (*i.e.* that happen once in a blue moon).[17] In principal, this has the advantage that simulations that follow

† E-mail: w.smith@daresbury.ac.uk

the reaction coordinate for diffusion can be carried out at ambient temperature, and thus sample all thermally accessible 'diffusive paths'. Adequately sampling points in phase space possessing low equilibrium populations (*e.g.* transition states or high-energy adsorption sites) presents no difficulty, as the simulation can be constrained to sample phase space around any point along the reaction path. The force required to satisfy this constraint can then be used to obtain the free energy of the adsorbate in the zeolite by integration along the reaction path, thus removing the need in TST theory to invoke the harmonic approximation to estimate entropy.

Bluemoon ensemble

The Bluemoon ensemble[17] was designed for studying activated processes in which the crossing of a potential barrier is an infrequent event on the timescale of other molecular and vibrational processes in the system. If the reaction path is known, the free energy profile for the process can be obtained from a series of simulations in which the reaction coordinate (ξ) is constrained to selected points along the pathway. The free energy W ($\xi^\dagger$) associated with a particular point ($\xi^\dagger$) on the reaction coordinate is obtained by integration of the corresponding force along ξ

$$W(\xi^\dagger) = \int_\infty^{\xi^\dagger} F(\xi)\,\mathrm{d}\xi \tag{1}$$

where the mean force $[F(\xi^\dagger)]$ to hold the system at the reaction coordinate $\xi = \xi^\dagger$ can be evaluated from:[17]

$$F(\xi^\dagger) = \frac{\langle(\partial \boldsymbol{r}/\partial\xi)\cdot[-\partial V/\partial \boldsymbol{r} + \beta^{-1}\,\partial \ln(|J|)/\partial \boldsymbol{r}]\delta(\xi(\boldsymbol{r}) - \xi^\dagger)\rangle}{\langle\delta(\xi(\boldsymbol{r}) - \xi^\dagger)\rangle} \tag{2}$$

where β is $1/kT$, $|J|$ the Jacobian determinant $|J| = |\partial \boldsymbol{r}/\partial \boldsymbol{q}|$, $\boldsymbol{r}$ Cartesian coordinates, $\boldsymbol{q}$ the coordinate system ($\bar{\boldsymbol{q}}$, ξ, σ) in which $\bar{\boldsymbol{q}}$ (with ξ) is a convenient set of generalised coordinates, and σ represents any constraint condition (such as fixed bond lengths *etc.*). As usual, in eqn. (2) the angular brackets $\langle\cdots\rangle$ indicate an ensemble average and δ is the Kronecker delta. The term involving $(\partial \boldsymbol{r}/\partial\xi)\cdot(\partial V/\partial \boldsymbol{r})$ is the generalised force, the derivative of potential energy in the direction of the reaction coordinate, and is the negative of the constraint force, F_c, required to enforce the constraint $\xi = \xi^\dagger$ in the simulation. The term involving $\ln(|J|)$ accounts for the apparent force that arises from the non-inertial (*e.g.* centrifugal) nature of ξ. This may only be determined if the reaction path is known. However, if ξ is a linear combination of the Cartesian coordinates this Jacobian term is exactly zero.

The probability density of $\xi^\dagger$, $P(\xi^\dagger)$, can be obtained from the free energy[17]

$$W(\xi^\dagger) = -\beta^{-1}\ln[P(\xi^\dagger)/P_u] \tag{3}$$

where P_u is the uniform density of $\xi^\dagger$.

The Bluemoon ensemble may also be used to obtain the rate at which barrier crossing occurs. If the transition state lies at $\xi(\boldsymbol{r}) = \xi^\ddagger$, we can define the 'reactant' side of the free energy profile to be those states with $\xi(\boldsymbol{r}) < \xi^\ddagger$ while the 'product' side is those states with $\xi(\boldsymbol{r}) > \xi^\ddagger$. If barrier crossing is an activated process then a timescale separation will exist between the crossing processes and other internal degrees of freedom of the system. The rate constant for crossing is given by the plateau value of $k(t)$[17] where:

$$k(t) = \langle\dot{\xi}\delta(\xi(\boldsymbol{r}) - \xi^\ddagger)\theta(\xi(\boldsymbol{r}) - \xi^\ddagger)\rangle/\langle\theta(\xi(\boldsymbol{r}) - \xi^\ddagger)\rangle \tag{4}$$

and θ is the Heavyside step function: $\theta(x) = 1$ if $x \geqslant 0$, and $\theta(x) = 0$ otherwise.

The TST rate constant is $k_{TST} = \lim_{t\to 0^+} k(t)$ and the time-dependent transmission coefficient $\kappa(t) = k(t)/k_{TST}$. For the system we examine, the TST rate constant may also be obtained from[17]

$$k_{TST} = (2\pi\beta\mu_{eff})^{-1/2}P(\xi^\ddagger)/\langle\theta(\xi(\boldsymbol{r}) - \xi^\ddagger)\rangle \tag{5}$$

where μ_{eff} is an effective mass. κ and related quantities are accessible by calculating appropriate correlation functions from a large number of independent and unconstrained simulations starting from states with $\xi(\boldsymbol{r}) = \xi^\ddagger$. The starting configurations for these simulations are generated from simulations in which the constraints $\xi(\boldsymbol{r}) = \xi^\ddagger$; $\dot{\xi} = 0$ were applied. The velocities $\dot{\xi}$ for the subsequent unconstrained simulations are then selected from a Maxwell–Boltzmann distribution.

In any event, evaluation of the rate constants and free energies can only be obtained once the reaction coordinate [and hence $\partial \boldsymbol{r}/\partial\xi$ in eqn. (2)] is known. To do this in the system under study we must first characterise the reaction path.

Parametrization of the reaction path

In general, any path in $\mathscr{R}^N$ can be described parametrically by the equation

$$\boldsymbol{p}(t) = [x_1(t), x_2(t), \ldots, x_N(t)|A \leqslant t \leqslant B] \tag{6}$$

where the parameters x_i are functions of the variable t and may be regarded as the components of the N-dimensional vector $\boldsymbol{p}$, which traces out the path between the limits A and B. As should be clear, for our purposes we require that the parameters x_i be continuous in the variable t and that all first and second derivatives exist. The length travelled along the path is the reaction coordinate, ξ, described in the previous section. The path length is found by integrating the magnitude of the derivative vector:

$$\xi(t) = \int_A^t |\boldsymbol{p}'(s)|\,\mathrm{d}s \tag{7}$$

In the system we study here, it transpires that we can always define the path in terms of a parametric curve in $\mathscr{R}^3$ using three parameters $\{x, y, z\}$, the Cartesian components of $\boldsymbol{p}$ with respect to the standard unit vectors $\{\hat{i}, \hat{j}, \hat{k}\}$. (In practice, this may not, however, be the most convenient frame of reference, see below.) Furthermore, if the paths are single valued on one parameter (x say) we can use $x(t) = t$, and replacing y by the symbol g and z by h we obtain the parametric curve in the form

$$\boldsymbol{p}(x) = [x, g(x), h(x)\,|\,A \leqslant x \leqslant B] \tag{8}$$

The reaction coordinate, ξ, is then obtained from eqn. (7) as

$$\xi(x) = \int_A^x \sqrt{[1 + g'(s)^2 + h'(s)^2]}\,\mathrm{d}s \tag{9}$$

where the prime ($'$) indicates a derivative with respect to the independent variable.

The reaction coordinate ξ defines one of the three generalised coordinates required by eqn. (2), the two remaining are defined in the transformation $(x, y, z) \to (\xi, \zeta, \lambda)$, where $\zeta = y - g(x)$ and $\lambda = z - h(x)$, from which it follows that

$$|J| = [1 + g'(x)^2 + h'(x)^2]^{-1/2} \tag{10}$$

and thus the components of $\partial \ln|J|/\partial(x, y, z)$ are

$$\frac{\partial \ln|J|}{\partial x} = \frac{1}{J}\frac{\mathrm{d}J}{\mathrm{d}x} = \frac{-g'(x)g''(x) - h'(x)h''(x)}{[1 + g'(x)^2 + h'(x)^2]} \tag{11}$$

and

$$\frac{\partial \ln|J|}{\mathrm{d}y} = \frac{1}{|J|}\frac{\partial|J|}{\partial y} = 0$$

$$\frac{\partial \ln|J|}{\partial z} = \frac{1}{|J|}\frac{\partial|J|}{\partial z} = 0 \tag{12}$$

In practice, in applying the above equations, it may be preferable to use parameters different from the Cartesian coordinates $\{x, y, z\}$ in which the simulation is performed, particularly in a crystalline solid, where certain directions have special significance. Then we may resort to alternative parameters $\{u, v, w\}$ referring to unit vectors $\{\hat{u}, \hat{v}, \hat{w}\}$ which are related to the standard set *via* a unitary transformation. Thus, for the straight channel in silicalite-1, we used $\hat{u} = (0, 1, 0)$, $\hat{v} = (0, 0, 1)$ and $\hat{w} = (1, 0, 0)$, and for the sinusoidal channel we used $\hat{u} = (-a, 0, c)/\sqrt{(a^2 + c^2)}$, $\hat{u} = (c, 0, a)/\sqrt{(a^2 + c^2)}$ and $\hat{w} = (1, 0, 0)$ (a and c being the lengths of the ***a*** and ***c*** unit cell vectors). Following transformation of the simulation results into one of these reference frames, the above equations may be applied with substitution of (u, v, w) for (x, y, z) respectively.

A convenient choice of reaction coordinate in the system under study is the position of the benzene centre of mass (COM). However, *a priori*, this is unknown and empirical determination of the path is required. In our simulations the benzene COM was constrained to lie in the plane perpendicular to $\hat{u}$ at $u = u^{\dagger}$ and averages were taken of the position of the COM in the $\hat{v}$ and $\hat{w}$ directions. Translations of the benzene were not constrained in the plane normal to $\hat{u}$, nor was any constraint applied to the rotational degrees of freedom. The averages obtained were thus a weighted average over all thermally accessible reaction paths that pass through the $u = u^{\dagger}$ plane. The reaction path obtained was therefore a 'mean' reaction path. Since the path along the channels is periodic, the fitting of the parametric functions $g(u)$ and $h(u)$ [eqn. (8)], as a function of u was achieved using a Fourier series. In each case, Fourier series components with wavelengths less than 1.0 Å were omitted from the fitting procedure.

A slight disadvantage of applying the constraint in the form $u = u^{\dagger}$ rather than $\xi = \xi^{\dagger}$ is that the calculation of the constraint force term $F_c = \partial V/\partial(u, v, w)$ [eqn. (2)] is a projection (F_u) in the direction of $\hat{u}$ and not the true constraint force term F_c. However, the fitting of the reaction path allows the calculation of the derivatives $g'(u)$ and $h'(u)$ and from these it is simple to obtain the other components of F_c, namely F_v and F_w in the directions $\hat{v}$ and $\hat{w}$, respectively, as:

$$F_v = F_u g'(u) \qquad F_w = F_u h'(u) \qquad (13)$$

from which F_c may be determined. The force F_c is to be regarded as the mean force associated with the mean reaction path. Once again, the constraint force F_c as a function of u can be fitted as a Fourier series in the same manner as the reaction path.

To conclude this section it should be noted that the reaction coordinate here is based entirely on the position of the benzene COM. This does not mean, however, that the rotational degrees of freedom are ignored. The computed reaction path is effectively an average over the thermally accessible orientational degrees of freedom. The model, consistent with the Bluemoon ensemble, thus assumes that, as the benzene diffuses along the reaction path, the molecule has sufficient time to sample adequately the orientations at each point. Experimentally, the rate of diffusion of benzene in silicalite is low ($D = 2.2 \times 10^{-10}$ cm^2 s^{-1})[18] and the rotational motion of benzene is on a timescale of the order of 1 ps. It follows that a reaction coordinate based on the benzene COM is adequate.

Molecular models

At low loadings of benzene, silicalite has an orthorhombic crystal structure with *Pnma* symmetry. The equivalent positions in this structure are (x, y, z), $(\bar{x} + \frac{1}{2}, \bar{y}, z + \frac{1}{2})$, $(\bar{x}, y + \frac{1}{2}, \bar{z})$, $(x + \frac{1}{2}, \bar{y} + \frac{1}{2}, \bar{z} + \frac{1}{2})$, $(\bar{x}, \bar{y}, \bar{z})$, $(x + \frac{1}{2}, y, \bar{z} + \frac{1}{2})$, $(x, \bar{y} + \frac{1}{2}, z)$ and $(\bar{x} + \frac{1}{2}, y + \frac{1}{2}, z + \frac{1}{2})$. The straight channels run along [010] with the intersection with the sinusoidal channels being at (0, 1/4, 1/2).

Two models of the silicalite lattice were used in this work. The first was a rigid ion, rigid lattice model which allows our results to be compared directly to other studies of this system in the literature. The second, more realistic, model, was the shell model potential of Schröder and Sauer.[19] Of all the current models available in the literature this model gave the best account of both structural and dynamic properties of the silicalite framework. In particular, the vibrational spectrum, phonon modes and elastic constants of this model were in very good accord with experimental values. Correctly describing these properties was expected to be important for this study, as distortions induced by the aromatic species in the zeolite framework were likely to be significant factors in the activation energy for passage of the benzene through the channel network.

The Schröder and Sauer potential contains electrostatic, repulsive and angular terms. In addition, each oxygen is described as a polarizable core–shell unit while the silicon atoms are treated as point ions. The potential energy has the form:

$$V = \sum_{i>j}\left[\frac{q_i q_j}{4\pi\varepsilon_0 r_{ij}} + A_{ij}\exp(-r_{ij}/\rho_{ij})\right] + \sum_{\text{angles}}\frac{k_\theta}{2}(\theta_\alpha - \theta_0)^2 + \sum_{\text{shells}}\frac{k_{\text{sh}}}{2}r_{\text{c–s}}^2 \qquad (14)$$

where q_i is atomic charge, r_{ij} the interatomic separation between sites i and j, and $r_{\text{c–s}}$ the core–shell separation. The prefactor (A_{ij}) of the repulsive term is non-zero only for Si–O_{shell} interactions, while the prefactor for the bond angle term, k_θ, is non-zero only for O_{shell}–Si–O_{shell} triplets in which both oxygen shells are in the first coordination sphere of the Si. Values of the force constants and other parameters are given in Table 1. The bond angle term is a three-body potential which, as well as contributing to the elastic properties of the lattice, helps to preserve the structural integrity of the lattice particularly under the stresses introduced by the presence of the benzene.

For benzene, an all-atom planar rigid model was used. The C—C bond length was 1.4 Å and the C—H bond length 1.09 Å. The benzene–zeolite potential interaction was that used in a number of previous studies by Snurr *et al.*[16,18,20] It consists of atom–atom interactions containing Lennard-Jones and Coulombic terms, values of which are given in Table 2. Note that the charges we used on the benzene sites were half those used by Snurr *et al.* because our zeolite sites had twice the

Table 1 Potential parameters for intra-zeolite interactions

	$q/\lvert e\rvert$	A_{ij}[a]	ρ_{ij}/Å	k_{shell}[b]	k_θ[c]	θ_0[d]
Si	4.0					
O_{core}	1.062 37			10 879.96		
O_{shell}	− 3.062 37					
Si–O_{shell}		149 643.9	0.300 17			
O_{shell}–Si–O_{shell}					17.7504	109.47

[a] Units of kJ mol^{-1}. [b] Units of kJ mol^{-1} Å^{-2}. [c] Units of kJ mol^{-1} rad^{-2}. [d] Units of degrees.

Table 2 Potential parameters for benzene–zeolite interactions

	$q_i/\|e\|$	A/kJ mol^{-1} Å^{12}	B/kJ mol^{-1} Å^{6}
C	−0.075		
H	0.075		
C–O$_{shell}$		1.335×10^6	1.807×10^3
H–O$_{shell}$		1.599×10^5	5.108×10^2

charge of their rigid ion and rigid lattice model. This benzene/silicalite model yields excellent agreement with experimental thermodynamic quantities (Henry's Law constants and isosteric heats of adsorption[20]) but the diffusion coefficients estimated from TST calculations in a rigid lattice are two orders of magnitude too low at 300 K.[16]

Computational methods

Bluemoon routines were implemented in the parallel molecular simulation package DL_POLY[21] and calculations performed on the 16 node IBM SP/2 at Daresbury laboratory. The simulations were conducted in the canonical ensemble with a Nosé–Hoover thermostat[22] with a relaxation rate of 1 ps^{-1}. The equations of motion were solved using a leapfrog scheme, with an implicit quaternion algorithm[23] used for the rigid benzene molecule. We used the dynamical shell model method of Fincham[24] to integrate the core–shell degrees of freedom. In this scheme some fraction of the oxygen mass is assigned to the shell and adiabatic molecular dynamics performed on the system. The partitioning of the mass is chosen so that the normal modes of the core–shell unit are decoupled from the rest of the system. We assigned 2 u of mass to each shell and 13.9994 u to each core, giving the core–shell unit a reduced mass, μ, of 1.75 u. The resonance wavenumber of the core–shell unit was thus $\bar{\nu} = 1/(2\pi)\sqrt{k_{sh}/\mu} = 4186$ cm^{-1}. This ensured the core–shell degrees of freedom were well decoupled from the rest of the system, since the next highest silicalite mode is around 1000 cm^{-1}.[19]

Paths along the straight and sinusoidal channels were computed with both a rigid and flexible zeolite lattice. In practice, a five-step procedure was followed to obtain the free energy profile for a particular channel:

1. Simulation: a series of constrained simulations was conducted in each of which the adsorbate was confined to a particular plane $\hat{\Upsilon} = \hat{\Upsilon}'$, with $\hat{\Upsilon}$ the *a priori* 'best guess' to the direction of the reaction path. (This was along [010] for the straight channel and [$\bar{1}$01] for the sinusoidal channel.) The position and magnitude of the constraint force in the direction $\hat{\Upsilon}$ was computed in each case.

2. Path construction: the mean adsorbate centre of mass positions from step 1 were used to construct the mean reaction path, ξ. This was done by first transforming the simulation data to the frame $\{\hat{u}, \hat{v}, \hat{w}\}$ by a unitary transformation, so that $\hat{\Upsilon} = \hat{u}$ (and the path was single valued and periodic on u). The v and w components of the COM position were then fitted as functions of u using a Fourier series. ξ was calculated as the distance travelled along the fitted path starting from $u = 0$ [eqn. (9)].

3. Jacobian calculation: the Jacobian term, $(\partial \mathbf{r}/\partial\xi)\cdot[\partial \ln(|J|)/\partial \mathbf{r}]$ in eqn. (2) was evaluated analytically from the fitted reaction path as a function of ξ.

4. Constraint force calculation: the positions and constraint forces (from step 1) were projected onto the ξ coordinate using eqn. (13). The forces, as a function of ξ, were fitted using a Fourier series. This ensured the fitted forces were periodic on ξ and that the integral over one periodic unit was exactly zero. (However, fitting of the forces to be periodic on u does not guarantee that the integral vanishes over one periodic length of ξ.)

5. Free energy calculation: the integral with respect to ξ in eqn. (1) was evaluated from the fitted constraint force (step 4) and the Jacobian term (step 3) to obtain the free energy, $W(\xi)$.

In all simulations the MD cell contained two unit cells of silicalite, stacked in the Z direction and with periodic boundary conditions applied in all three directions. The short-ranged pair potential terms were truncated at 9.8 Å and the electrostatic terms calculated using Ewald summation[25] with energies and virial converged to 1 part in 10^5.

The zeolite structure used for the rigid framework simulations was taken from ref. 26. The basic unit cell was orthorhombic with cell lengths of $a = 20.022$ Å, $b = 19.899$ Å and $c = 13.383$ Å. The Schröder and Sauer shell-model potential had slightly different cell parameters, which we obtained from averaging over 100 ps of NPT simulations at 300 K and 0 kbar. This also produced an orthorhombic cell with *Pnma* symmetry but with dimensions of $a = 20.318$ Å, $b = 20.171$ Å and $c = 13.585$ Å.

The choice of time step was limited by the highest frequency mode in the system (*i.e.* oscillations of the core–shell unit in the flexible zeolite). We used 1.2 fs time step simulations using the shell-model potential for the zeolite and a 12 fs time step with the rigid lattice. Rigid lattice simulations were typically 50 ps duration including a 5 ps equilibration period. Flexible lattice simulations were typically 30 ps duration with a 5 ps equilibration period.

In each series of constrained simulations for a given channel the starting configuration for each simulation was constructed from the final configuration of the previous simulation in the series. The benzene COM was repositioned to its mean position from the previous simulation and shifted by typically 0.1 Å to 0.25 Å in the Υ direction.

Statistical uncertainties in the position and constraint force upon the benzene were evaluated using the blocking technique of Jacucci and Rahman.[27] Typically, the uncertainty in the unconstrained components of position was ±0.02 Å and the uncertainty in the components of the constraint force ±0.3 kJ mol^{-1}. The two components of the mean constraint force in the constraint plane were always zero, to within statistical uncertainty. The statistical correlation time for the forces in the constrained simulations of the flexible zeolite was typically 70 fs, implying that in the 20 ps of simulation used for collecting statistics there were *ca.* 280 completely independent measurements of the constraint force. However, near positions corresponding to a maximum in the absolute force, the correlation time was typically twice this value and the statistical uncertainty associated with each average correspondingly higher.

Results

Straight channel

Reaction path. The straight channel runs approximately in the [010] direction, with the asymmetric cell unit in the region $0 \leqslant y \leqslant b/4$. To assess statistical reliability of the data we carried out simulations in two asymmetric cell units, *viz.* in the region $0 \leqslant y \leqslant b/2$. The mean benzene position as a function of the y coordinate in rigid silicalite is shown in Fig. 2, together with the fitted functions used to define the reaction path. The path shows only minor deviation from $x = 0$ but deviation from $z = -c/2$ is more noticeable, particularly in the vicinity of $y = b/4 \approx 5$ Å. This region is where the straight channel intersects with the sinusoidal channels. The maximum distance that the benzene 'drops' into the channel intersection from $z = -c/2 = -6.6915$ Å on the fitted path is $\Delta z = 1.324$ Å. (This quantity will be relevant when we discuss the path for diffusion in the sinusoidal channel.) The channel intersection (between $y \approx 3$–7 Å) is where the x component is also most poorly characterised, since in this region the benzene is considerably less confined than when in the channels themselves. As will be seen, this region was the most favoured adsorption

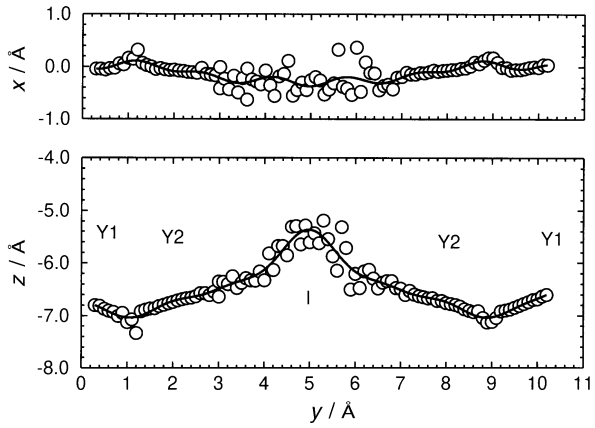

Fig. 2 Parametrization of the path in the X and Z directions as a function of Y for benzene in the straight channel of rigid silicalite. The circles represent data from the simulations and the solid line the best-fit path through the points. I, Y1 and Y2 label the approximate position of minima in the free energy of the system.

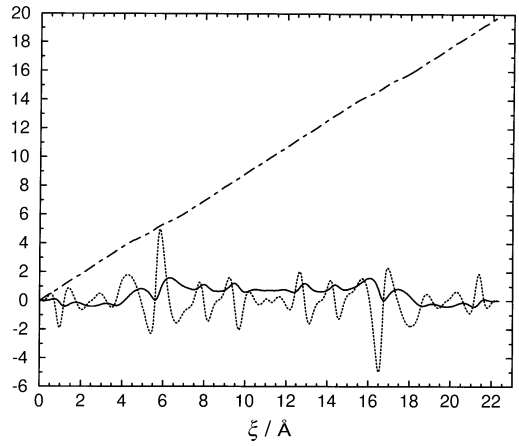

Fig. 3 Reaction coordinate and Jacobian terms for the straight channel of rigid silicalite. The data shown are: y (Å) as a function of ξ (–·–), the Jacobian term $RT[\partial(x, y, z)/\partial\xi]$ $[\partial \ln(|J|)/\partial(x, y, z)]$ in units of kJ mol^{-1} Å^{-1} (····), and integral of the Jacobian term, in units of kJ mol^{-1}, (——).

site in the zeolite framework.

The total path length along one unit cell length was found, from eqn. (9), to be 22.32 Å. This is 12% longer than a direct path along [010]. The non-inertial force, and its integral, arising from the non-linear nature of ξ is shown in Fig. 3. The forces as a function of ξ were fitted to a Fourier series on ξ (Fig. 4). The free energy profile obtained from applying eqn. (1) and (2) is shown in the same figure. It is apparent that, in this case, the Jacobian terms have only a small effect on the free energy profile of the system. Consistent with previous studies,[15] three distinct adsorption sites were located in the straight channel. The first (I) is near the intersection with the sinusoidal channels, the second (Y1) is midway between adjacent I sites. The third site (Y2), lies approximately midway between adjacent Y1 and I sites. The locations and relative free energies of these adsorption sites and of the transition states (maxima) between these sites are given in Table 3.

The same procedures were also applied to the flexible lattice. In this case the reaction path (not shown), scaled to account for the slight change in cell parameters, was very similar to that obtained for rigid silicalite. However the forces, and hence the free energies (Fig. 4), were approximately half those obtained with the rigid zeolite potential. Consequently the free energy of activation for diffusion from I into the channel was *ca.* 30 kJ mol^{-1} lower (Table 3) than for the rigid lattice.

Calculation of the transmission coefficient. The transmission coefficient, κ, is the fraction of trajectories passing through the transition state that succeed in crossing the barrier. This can be determined directly in the Bluemoon ensemble by calculating the correlation function

$$\kappa(t) = \frac{\langle \dot{\xi}(t=0)\delta(\xi(t=0)-\xi^{\ddagger})\theta(\xi(t)-\xi^{\ddagger})\rangle}{\langle \delta(\xi(t=0)-\xi^{\ddagger})\rangle} \qquad (15)$$

and evaluating the value of κ in the plateau region for times that are 'long' on the timescale of barrier crossing but 'short' on the timescale of the activated processes. To evaluate κ for passage from the channel intersection into the straight channel in flexible silicalite we generated 220 separate configurations equilibrated under the constraint $\xi = \xi^{\ddagger}$, where $\xi^{\ddagger}$ refers to the maximum in the free energy profile (Fig. 4) for I↔Y2. Configurations were written out every 0.36 ps. Each configuration was then run forwards in time in the unconstrained ensemble with the y-component of the benzene COM velocity selected from the Maxwell–Boltzmann distribution at 300 K and chosen so the molecule was initially moving towards the Y2 site. Each simulation was 10 ps in length. The plateau value of κ obtained (Fig. 5) for this barrier crossing is 0.75 ± 0.04. The oscillations in the figure corresponds to recrossing events, most of which occur within 2 ps of the molecule crossing the top of the barrier.

Table 3 Free energy, (W/kJ mol^{-1}), of minima and maxima for benzene in the asymmetric unit cell of silicalite at 300 K

	rigid		flexible	
	position	W	position	W
straight channel				
min. I	(0.019, 0.25, −0.401)	0.00	(0.018, 0.250, −0.410)	0.00
min. Y1	(0, 0, −0.5)	31.70	(0, 0, −0.5)	11.91
min. Y2	(0.003, 0.094, −0.505)	41.56	(0.003, 0.094, −0.513)	20.70
max. I↔Y2	(0.009, 0.145, −0.488)	60.53	(0.009, 0.144, −0.496)	27.62
max. Y2↔Y1	(−0.006, 0.055, −0.526)	55.64	(−0.005, 0.053, −0.533)	25.31
sinusoidal				
min. I	(−0.028, 0.25, −0.377)	0.00	(0.027, 0.25, −0.534)	0.00
min. S1	(−0.254, 0.25, −0.362)	53.03	(−0.251, 0.25, −0.365)	12.38
min. S2	(−0.340, 0.25, −0.362)	66.91	(−0.343, 0.25, −0.366)	15.90
min. S3	(−0.153, 0.25, −0.338)	56.12	(−0.155, 0.25, −0.351)	20.67
min. S4	(−0.437, 0.25, −0.264)	80.46	(−0.442, 0.25, −0.272)	26.24
max. I↔S4	(−0.448, 0.25, −0.223)	92.20	(−0.455, 0.25, −0.214)	34.17
max. S4↔S2	(−0.401, 0.25, −0.317)	100.70	(−0.425, 0.25, −0.304)	28.03
max. S2↔S1	(−0.289, 0.25, −0.379)	90.81	(−0.301, 0.25, 0.379)	20.27
max. S1↔S3	(−0.197, 0.25, −0.343)	108.19	(−0.182, 0.25, −0.310)	30.06
max. S3↔I	(−0.105, 0.25, −0.361)	81.64	(−0.109, 0.25, −0.358)	28.60

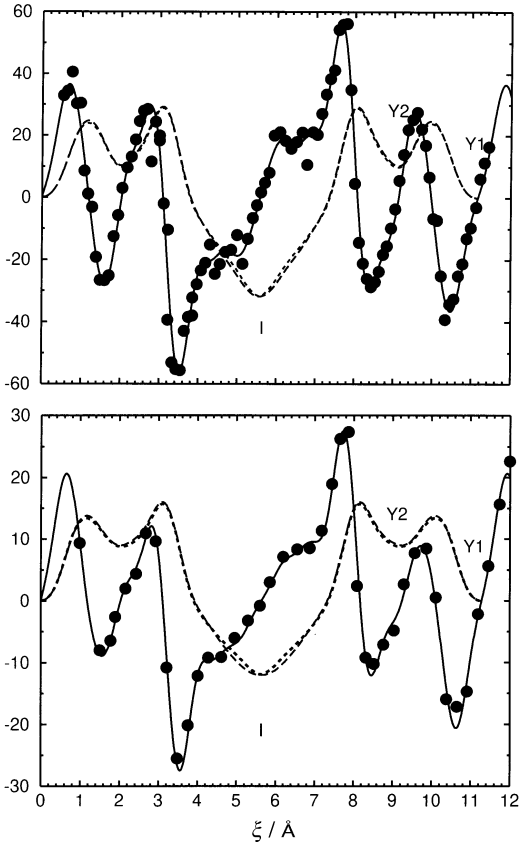

Fig. 4 Free energy and associated forces for benzene diffusion in the straight channel of rigid (top) and flexible (bottom) silicalite. Constraint forces (●), fitted force (——). The free energy, W (· · · ·) and the integral of the force [ignoring the Jacobian terms in eqn. (2)] (– – –) are also shown. Energies are in units of kJ mol^{-1} and forces in units of energy/Å. I, Y1 and Y2 label the same points as in Fig. 2.

Sinusoidal channel

The techniques used to study the straight channel were applied to the sinusoidal channel with only minor modification. In this case the channel in the XZ plane follows a zigzag path (Fig. 1), though each branch of the path is equivalent by symmetry. The first branch of the channel follows the direction [$\bar{1}$01] until the intersection with the straight channel and thereafter follows the direction [$\bar{1}0\bar{1}$]. The direction [$\bar{1}$01] was chosen for the simulations.

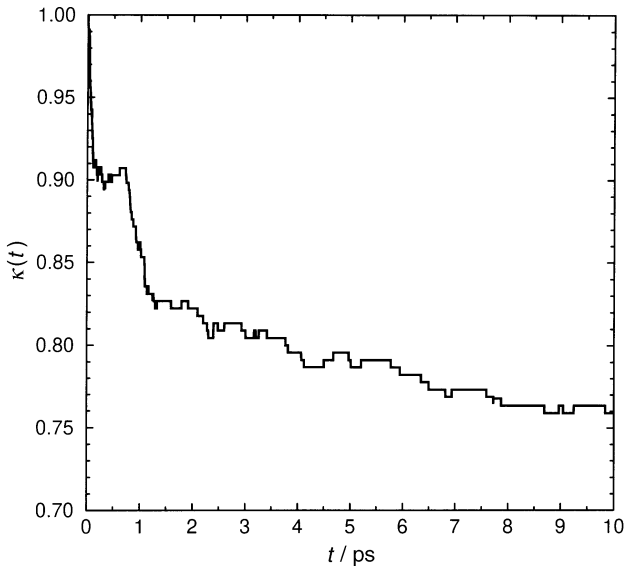

Fig. 5 Evaluation of the transmission coefficient for passage from the channel intersection into the straight channel in flexible silicalite

The mean COM positions in the XZ plane for one branch of the channel are shown in Fig. 6. Also shown are the symmetry equivalent positions for the second branch. The y component of the mean COM position was always $b/4$ within statistical uncertainty and consequently all subsequent analysis assumed y was fixed at this value. The points that lay outside the interval $-0.6 > x/\text{Å} > -10.6$ (*i.e.* where the raw data and the symmetry equivalent points cross in Fig. 6) were then discarded, since these simply correspond to the benzene meeting up with the channel wall at the end of a segment of the channel. The resulting reduced set of points were then fitted.

The vector $\boldsymbol{u}$ used for the fit of the reaction path was $\boldsymbol{u} = (-a/2,\ 0,\ c_{\text{eff}})$ where $c_{\text{eff}} = c/2 - 2\Delta z$. This was close to the 'best guess' vector used in the simulations, but allowed for the benzene COM 'dropping' in the c direction at the intersection of the straight and sinusoidal channels (points I in Fig. 6), as was observed in the straight channel case. From Fig. 6, we estimate $c_{\text{eff}} = 3.6$ Å, which gives $\Delta z = 1.55$ Å. This is 0.2 Å larger than the value obtained from the straight channel study, indicating the difficulty in locating the precise mean path through the pore intersection which, in free energy terms, contains a rather broad minimum. Unlike the straight channel, the sinusoidal channel has no centre of symmetry and hence the Fourier series used to describe the function $g(u)$ was

$$g(u) = -c_0 + \sum_{k=1}^{7} c_i \sin\left[\frac{2k\pi}{d}u\right] + d_i \cos\left[\frac{2k\pi}{d}u\right] \quad (16)$$

where $d = \sqrt{([a/2]^2 + c_{\text{eff}}^2)} = 10.638$ Å, is the direct distance between the I sites. The total path length from site to site is 14.273 Å, 34% longer than if a straight path were assumed. The fitted reaction path is shown in Fig. 6, plotted as a function of u and v, where $\boldsymbol{v}$ is a vector orthogonal to $\boldsymbol{u}$ in the XZ plane.

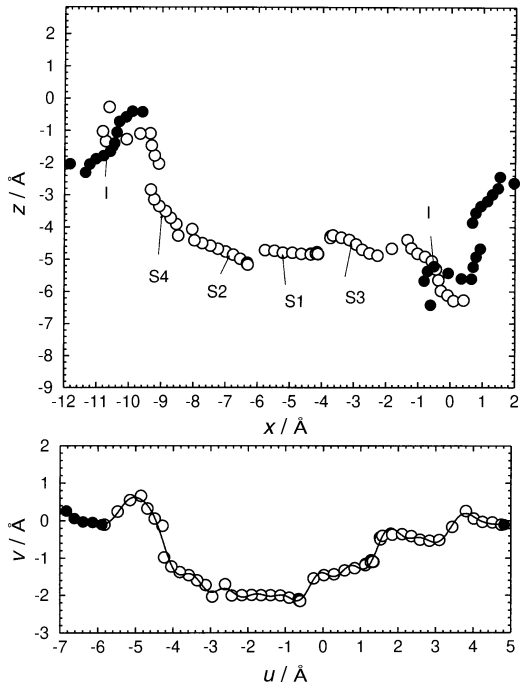

Fig. 6 (Top) Mean benzene COM position in the sinusoidal channel of rigid silicalite. Simulation data (○) and symmetry equivalent points (●) are shown. I, S1, S2, S3 and S4 label positions of free energy minima (see text for details). (Bottom) Mean benzene COM position in rigid silicalite in transformed coordinates, u and v. u runs in the direction between the I sites, with v orthogonal in the XZ plane. The fitted path is shown as a solid line.

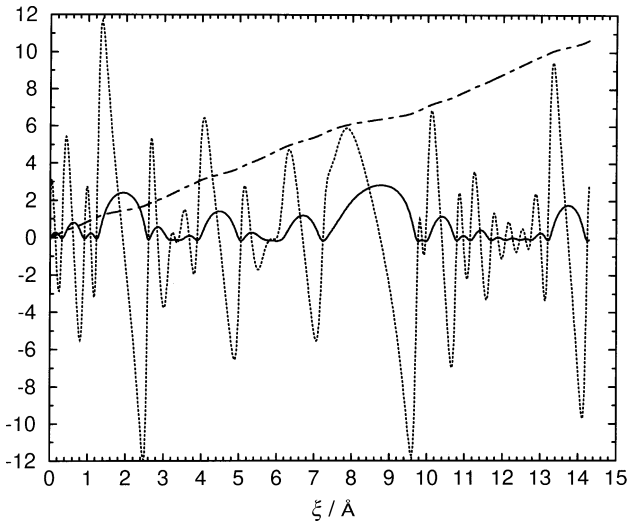

Fig. 7 Reaction coordinate and Jacobian terms for the sinusoidal channel of rigid silicalite. The data shown are: u (Å) as a function of ξ (– · –), the Jacobian term $RT[\partial(u, v)/\partial\xi]$ $[\partial \ln(|J|)/\partial(u, v)]$ in units of kJ mol^{-1} Å^{-1} (· · · ·), and integral of the Jacobian term, in units of kJ mol^{-1} (——).

Evaluation of the Jacobian (Fig. 7) and the free energy (Fig. 8) was straightforward. We found four distinct adsorption sites in the sinusoidal channel (labelled S1–S4 in Fig. 8). The positions and energies of these sites, and of the transition states connecting them are given in Table 3. The Jacobian terms have a larger influence on the free energy profile than for the straight channel. Although the positions of the maxima and minima are relatively unaffected by neglect of these terms;

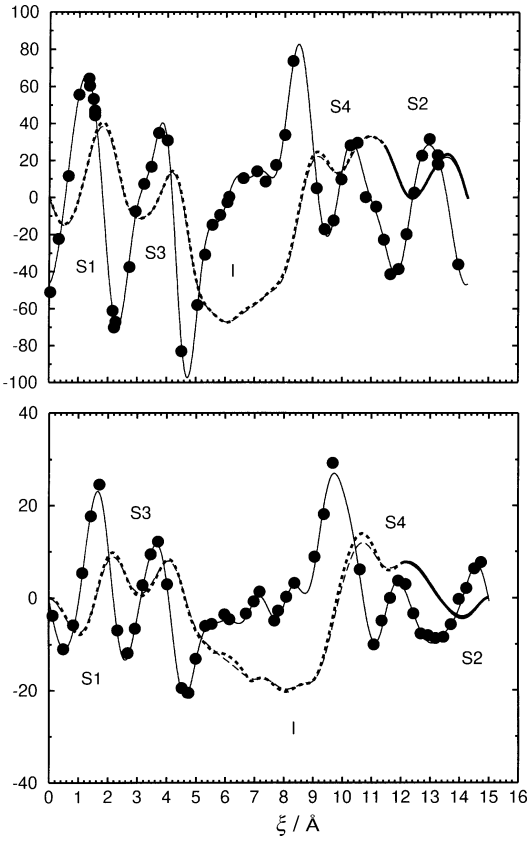

Fig. 8 Free energy profile and associated force for benzene in the sinusoidal channel of rigid (top) and flexible (bottom) silicalite. Annotation as in Fig. 4.

Table 4 Equilibrium populations of adsorption sites at 300 K

site	n_i	p_i (rigid)	p_i (flexible)
I	1	1.000	0.982
Y1	1	3.02×10^{-6}	8.29×10^{-3}
Y2	2	1.16×10^{-7}	4.89×10^{-4}
S1	1	5.8×10^{-10}	6.87×10^{-3}
S2	1	2.2×10^{-12}	1.67×10^{-3}
S3	1	1.7×10^{-10}	2.47×10^{-4}
S4	1	9.8×10^{-15}	2.65×10^{-3}

they make at most a 3 kJ mol^{-1} (for I↔S4 near $\xi = 9$ Å) contribution to the free energy of the transition states.

Analysis of the results for the sinusoidal channel of the flexible silicalite followed the same procedure as for the rigid case. In this case, the key parameters are: $d = 11.799$ Å, $\Delta z = 0.40$ Å, and the path length between I sites, $\xi = 15.01$ Å. The corresponding free energy plot is also presented in Fig. 8. As with the rigid lattice four adsorption sites, in addition to the I site, are found for the sinusoidal channels. Inclusion of flexibility in the zeolite had several important effects. First, as for the straight channel, the free energy differences between sites were considerably lower than with a rigid lattice. Secondly, the S2 site was lower in energy than S3 (Table 3). Thirdly, apart from the uncertainty in the location of I, only S3 and S4 were shifted to any degree from the positions in the rigid lattice. The shifts were about 0.2 and 0.1 Å, respectively, and occurred primarily in the z direction. The transition states near these maxima were also shifted by similar amounts.

Equilibrium populations and rate constants

The relative population of each adsorption site is

$$p_i = \exp(-W_i/RT)/\sum_i n_i \exp(-W_i/RT) \qquad (17)$$

where n_i is the degeneracy of the site. The populations of the various sites is given in Table 4 assuming the I site found in the studies of the straight channel is essentially the same site found in studies of the sinusoidal channel. Our estimates for the populations of the higher-energy sites are lower than other studies with the same potential model. Snurr *et al.*[16] report $p_Y = 8 \times 10^{-4}$ for (Y1 + 2 Y2) and $p_S = 3 \times 10^{-4}$ for (S1–S4) from evaluating the configurational integrals within the harmonic approximation. Direct Monte Carlo simulation[18] predicts values three–four times higher than these. In general, our results predict free energies for Y1 and Y2 that are 14 kJ mol^{-1} higher in energy relative to I than Snurr *et al.* and 33 kJ mol^{-1} higher in energy for (S1–S4).

Our rate constants for barrier crossing were obtained for the flexible zeolite only. These were obtained using eqn. (4) and are given in Table 5. For this, we assumed only three adsorption sites: I, Y = Y1 and S = S1. This is permissible because the barriers between Y2 and Y1 and between the S sites are much lower than the barriers connecting the channel to the pore intersection. The transition state for I → Y was taken as I↔Y2. The rate constants for passage between I and S were obtained by assuming the transmission coefficient κ

Table 5 Rate constants (s^{-1}) for barrier crossing of benzene in silicalite at 300 K

	k
I → Y1	2.3067×10^{6}
Y1 → I	2.7333×10^{8}
I → S1	1.1068×10^{6}
S1 → I	1.5834×10^{8}

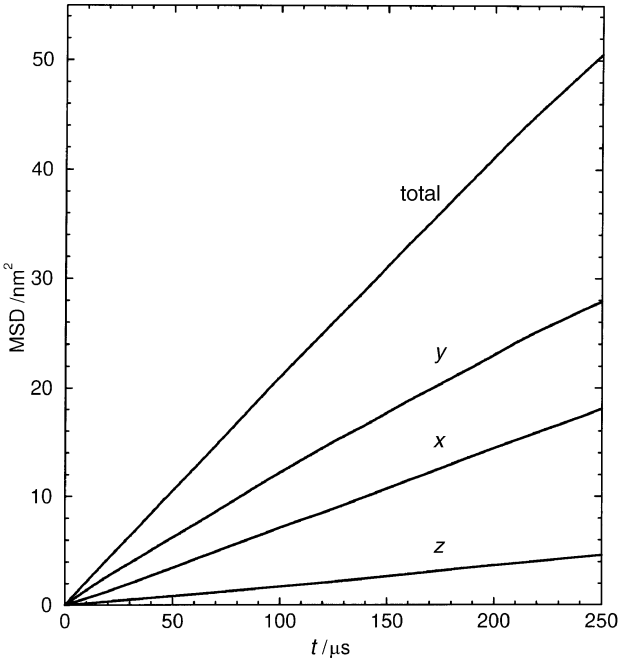

Fig. 9 Mean-squared displacements of benzene in silicalite at 300 K as obtained from lattice Monte Carlo simulation. The calculations used a single benzene molecule on a lattice with 125 000 time origins to evaluate the averages in eqn. (22).

was the same as for passage into the straight channel *viz*. 0.75. In fact, for I → S, two routes with different activation energies are possible. The value for $k_{I\rightarrow S}$ in Table 5 is the mean of these two rate constants where we have used the transition state S1 ↔ S3 for the route I → S3 → S1 and the transition state I ↔ S4 for the route I → S4 → S2 → S1. The rate for the reverse directions is given by the standard relationship between equilibrium populations and rate constants:

$$p_A/p_B = k_{B\rightarrow A}/k_{A\rightarrow B} = \exp([W_B - W_A]/RT) \tag{18}$$

Diffusion coefficients

Following June *et al.*[28] we have used the rate constants obtained above in lattice Monte Carlo simulations to determine the diffusivity. In these simulations a single benzene molecule was moved around a discrete three-dimensional matrix with points on the matrix corresponding to the I, Y and S sites in silicalite. The probability, $\rho_A(\tau)$, for the molecule at site A at time t to move to another site by time $t + \tau$ is governed by first-order kinetics:

$$\rho_A(\tau) = 1 - \exp(-k_A\tau) \tag{19}$$

where k_A is the sum of the rate constants for all possible processes:

$$k_A = \sum_B k_{A\rightarrow B} \tag{20}$$

The k_A are thus $k_I = 2(k_{I\rightarrow Y} + k_{I\rightarrow S})$, $k_Y = 2k_{Y\rightarrow I}$ and $k_S = 2k_{S\rightarrow I}$. When a move takes place, the probability the molecules moves to a specific site B is

$$\rho_B = k_{A\rightarrow B}/k_A \tag{21}$$

Our algorithm was as follows. First, a fixed time step, τ, was chosen to characterise the timescale for the diffusion process in the simulation. The average time for a transition from one site to another to occur is $\langle\tau_A\rangle = 1/k_A$. In our Monte Carlo simulation we therefore used a time step corresponding to one half the smallest of the $\langle\tau_A\rangle$ namely $\tau = \frac{1}{2}\langle\tau_S\rangle = 0.915$ ns. Next, at each time step a random number ζ_1 was selected from a uniform distribution on [0, 1). If ζ_1 was less than ρ_A the molecule was moved to a neighbouring lattice site. If the current site was I, then the molecule was moved into either an S or Y site, by selection based on another random variable, ζ_2. The molecule was thus moved to a Y site if ζ_2 was less than $2k_{I\rightarrow Y}/k_A$ and to an S site otherwise. If the current site was Y or S the molecule was moved to a neighbouring I site but with two equally probable directions for the move. Thus, a third random variable ζ_3 was selected on [0, 1) and the molecule moved in one direction if $\zeta_3 < 0.5$, and in the opposite direction otherwise. At the end of each time step the position of the molecule in the lattice was calculated. The diffusion coefficients, which are the diagonal elements of the diffusion tensor, were evaluated from the limiting slope of mean squared displacements *vs.* time:

$$D_{\alpha\alpha} = \lim_{t\rightarrow\infty} \frac{1}{2}\frac{\mathrm{d}\langle[r_\alpha(t) - r_\alpha(0)]^2\rangle}{\mathrm{d}t} \tag{22}$$

where the $\langle\cdots\rangle$ denotes an ensemble average, α labels the Cartesian directions (x, y or z) and $r_\alpha(t)$ is the α component of position at time t. The isotropic diffusion coefficient is the trace of the diffusion tensor:

$$D = \frac{D_{xx} + D_{yy} + D_{zz}}{3} \tag{23}$$

The simulation was 20 million steps (0.0183 s) in length. Previous studies[16,28] using similar techniques have used several hundred molecules and a variable time step determined by which sites the molecules find themselves in. However, by using a fixed time step we can considerably reduce the statistical uncertainty in determination of the $D_{\alpha\alpha}$, as all possible time origins in the simulation can potentially be used in the ensemble average of eqn. (22). Fig. 9 shows the mean-squared displacements obtained in our simulation evaluated out to 150 μS. The estimated diffusion coefficients are given in Table 6 and are in excellent agreement with the best estimate based on experimental measurements of $D = 2.2 \times 10^{-10}$ cm^2 s^{-1}.[18] We note, however, that experimental determinations of diffusion are subject to broad uncertainties and the observed agreement may be fortuitous.

The statistical accuracy of the Monte Carlo results can be gauged by realising that diffusion in the z direction can only occur by a series of moves involving both the straight and sinusoidal channels. Kärger[29] has derived the relationship

$$\frac{c^2}{D_{zz}} = \frac{a^2}{D_{xx}} + \frac{b^2}{D_{yy}} \tag{24}$$

assuming that the 'memory-function' of the benzene is short compared with the mean time of migration from one channel intersection to another. The value of D_{zz} so obtained from D_{xx} and D_{yy} is also given in Table 6 and agrees, within statistical uncertainty, with that obtained directly from the simulation.

Table 6 Diffusion coefficients (10^{-14} m^2 s^{-1}) of benzene in silicalite at 300 K

	D	D_{xx}	D_{yy}	D_{zz}
flexible	3.36	3.65	5.45	0.96
eqn. (24)				0.98
expt.	2.2			

Conclusions

The Bluemoon ensemble has been applied to the problem of benzene diffusion in silicalite as a pertinent example of an activated process for which empirical determination of the reaction path is required. In good accord with previous experimental and theoretical work, we find a number of clearly defined adsorption sites in the straight-channel intersection, the sinusoidal channel and at the intersection of these. Rate constants for hops between the adsorption sites separated by high barriers have been obtained and used in Monte

Carlo diffusion simulations to obtain the diffusion of benzene in a flexible model of silicalite at 300 K. The value obtained is in excellent agreement with experiment, and particularly so considering the diffusion constant is five orders of magnitude smaller than that normally observed in simple liquids (the usual domain for using MD to obtain diffusion coefficients).

The comparison of the different rigid lattice methods has revealed some interesting differences. Our estimate of the populations of the various adsorption sites in the rigid lattice are significantly lower than previous studies using the same potentials.[16,18] The implication is that our free energy differences (and generalised forces) are significantly too large in the rigid lattice. The crucial aspect is the characterisation of the reaction path and forces between the channel intersection and the first adsorption sites in the channel. Encouragingly however the rigid lattice simulations do yield essentially the same positions for free energy maxima and minima in the system and thus may be of some use in preliminary studies of adsorption and shape selectivity in higher aromatics.

However, it is clear that inclusion of zeolite flexibility has a strong effect on the free energy profile in comparison with rigid models and, hence, on the equilibrium populations of the sites and the height of the barriers for activated hops between them. This is not unexpected because the kinetic diameter of benzene is very close to the internal diameter of the channels and lattice relaxation and distortion effects must be important. The excellent agreement with experimental results for a flexible lattice supports this conclusion.

We are pleased to acknowledge support of T.R.F. from the former Science and Materials Computing Committee of the EPSRC. The simulations were performed on the IBM SP/2 parallel computer at Daresbury Laboratory. The advice and encouragement of Prof. G. Ciccotti, the Collaborative Computational Project CCP5 under Dr. M. P. Allen and the UK HPCI Materials Consortium under Prof. C. R. A. Catlow is also gratefully acknowledged.

References

1 J. Wei, *J. Catal.*, 1982, **76**, 433.
2 D. M. Ruthven, *Stud. Surf. Sci. Catal.*, 1995, **97**, 223.
3 H. J. Thamm, *J. Phys. Chem.*, 1987, **91**, 8.
4 C. Förste, A. Germanus, J. Kärger, H. Pfeifer, J. Caro, W. Pilz and A. J. Zikanova, *J. Chem. Soc., Faraday Trans. 1*, 1987, **83**, 2301.
5 H. Jobic, M. Bee and A. J. Dianoux, *J. Chem. Soc., Faraday Trans. 1*, 1989, **85**, 2525.
6 J. B. Nicholas, F. R. Trouw, J. E. Mertz, L. E. Iton and A. J. Hopfinger, *J. Phys. Chem.*, 1993, **97**, 4149.
7 K. S. Smirnov, *Chem. Phys. Lett.*, 1994, **229**, 250.
8 E. Hernández and C. R. A. Catlow. *Proc. R. Soc. London, Ser. A*, 1995, **448**, 143.
9 D. B. Shah, D. T. Hayhurst, G. Evanina and C. J. Guo, *AIChE J.*, 1988, **34**, 1713.
10 N. Van den Begin, L. V. C. Rees, J. Caro and M. Bülow, *Zeolites*, 1989, **9**, 287.
11 D. Shen and L. V. C. Rees, *Zeolites*, 1991, **11**, 666.
12 A. K. Nowak, A. K. Cheetham, S. D. Pickett and S. Ramdas. *Mol. Simul.*, 1987, **1**, 67.
13 O. Talu, *Mol. Simul.*, 1991, **8**, 119.
14 F. Vigné-Maeder and H. Jobic, *Chem. Phys. Lett.*, 1990, **169**, 31.
15 K-P. Schröder and J. Sauer, *Z. Phys. Chem.* (*Leipzig*), 1990, **271**, 489.
16 R. Q. Snurr, A. T. Bell and D. N. Theodorou. *J. Phys. Chem.*, 1994, **98**, 11948.
17 E. A. Carter, G. Ciccotti, J. T. Hynes and R. Kapral, *Chem. Phys. Lett.*, 1989, **156**, 472.
18 R. Q. Snurr, A. T. Bell and D. N. Theodorou, *J. Phys. Chem.*, 1994, **98**, 5111.
19 K-P. Schröder and J. Sauer, *J. Phys. Chem.*, 1996, **100**, 11043.
20 R. Q. Snurr, A. T. Bell and D. N. Theodorou, *J. Phys. Chem.*, 1993, **97**, 13742.
21 W. Smith and T. R. Forester, *Mol. Graphics*, 1996, **14**, 136.
22 W. G. Hoover, *Phys. Rev. A*, 1985, **31**, 1695.
23 D. Fincham, *Mol. Simul.*, 1992, **8**, 165.
24 D. Fincham and P. J. Mitchell, *J. Phys. Condens. Matter*, 1993, **5**, 1031.
25 M. P. Allen and D. J. Tildesley, *Computer Simulation of Liquids*, Clarendon Press, Oxford, 1989.
26 K. van Koningsveld, H. van Bekkum and J. C. Jansen, *Acta Crystallogr. Sect. B.*, 1987, **43**, 127.
27 G. Jacucci and A. Rahman, *Nuovo Cim. D*, 1973, **4**, 341.
28 R. L. June, A. T. Bell and D. N. Theodorou, *J. Phys. Chem.*, 1991, **95**, 8866.
29 J. Kärger, *J. Phys. Chem.*, 1991, **95**, 5558.

Paper 7/02063E; *Received* 25*th March*, 1997